DOI: 10.13009/EUCASS2019-839

The Hyperfine Structure of the OH* Emission Spectrum and its Benefits for Combustion Analysis

Robert Stützer and Michael Oschwald
DLR – German Aerospace Center, Institute of Space Propulsion
Im Langen Grund 1, D-74239 Hardthausen, Germany, Robert.Stuetzer@DLR.de

Abstract

The hyperfine structure of the OH radical emission spectrum was used to derive hydrogen flame temperatures in a research rocket combustor. A spectral resolution of less than 1nm was realized, revealing single molecular emission lines. Hence, relative intensities of several emission lines in the ultraviolet regime were investigated regarding temperature. Two groups of lines were used in order to correlate values of heat release with band intensities. Using an optically accessible diagnostic element, optical fiber, and a high-resolution spectrograph, measurements were conducted during LOX/gH2 combustion runs at the European research test bench P8. The feasibility of line-of-sight flame temperature measurements in the vicinity of the injector element was shown. Temperature values of (3200±200)K were determined. Experimentally obtained values are in good agreement with simulation data.

1. Introduction

This paper explains the results of optical measurements, obtained during a combustion chamber test campaign at the European Research test bench P8 (DLR Lampoldshausen, Germany). Using gaseous hydrogen fuel and liquid oxygen in the water cooled combustion chamber D (*BKD*), the test campaign HF4 aimed on investigations of high frequency combustion instabilities. Therefore, optical probes as well as pressure sensors were applied to the combustor for synchronous measurements. Flame temperature determination is a powerful tool to evaluate combustion efficiency and performance. Optical spectroscopy offers a variety of possibilities for contactless flame temperature measurements. Since the work of Dieke and Crosswhite [1] the hyperfine structure of the OH* flame emission spectrum is known and well-investigated. Pellerin *et al.* [2] developed a method to evaluate flame temperature values taking into account the intensity increase of several emission lines. In order to resolve single atomic transition lines, a Czerny-Turner-spectrograph with a grating of 3600 gr./mm was applied, retrieving a sub-nanometer spectral resolution.

2. Experimental

Test campaign “HF4” aimed on investigations of high frequency combustion instabilities. It was conducted at the European Research and Technology Test Bench P8 [3], located at the DLR Institute of Space Propulsion. Several test runs with gaseous as well as liquid hydrogen fuel and liquid oxygen were carried out using the model research combustor *D* (BKD) [4,5]. This water cooled combustion chamber was designed for pressures up to 80 bar and is equipped with a measurement ring that allows optical access into the injection zone of the combustion chamber. Furthermore, it possesses 8 dynamic pressure sensors, 4 thermocouples, 2 static pressure sensors, and 10 optical probes (Figure 1b). The combustor was chemically ignited. The injector head consists of 42 shear coaxial injectors which are variable in length in order to alter eigenfrequencies for the investigation of their effects on the chamber frequencies. Oxygen is injected at supercritical pressures, and the operating conditions are representative of modern flight engines using the propellant combination hydrogen/oxygen. The cylindrical combustion-chamber segment has a diameter of 80 mm and a nozzle-throat diameter of 50 mm.
For optical investigation, the measurement ring depicted in Figure 1b is installed between the injector head and the cylindrical segment. It is equipped with fiber-optical probes [5,6]. A small sapphire rod is mounted at the tip of the optical probe to create the optical access. Behind the the sapphire rod, the radiation is captured by an optical fiber connected to a Czerny-Turner-type Princeton Instruments SP-2750 spectrometer (focal length: 750 mm) and

DOI: 10.13009/EUCASS2019-839

recorded by a PI-MAX intensified camera (1024 × 256 active pixels, front illuminated, Peltier-cooled CCD). The fiber is a high-OH silica fiber with low attenuation in the UV and visible range. The full acceptance angle of the combustion chamber, the field of view can be approximated as a line. For the test runs presented here, the spectrometer is connected to optical probe number 4, as shown in Figure 1b. It is alligned to an injector on the second ring of the injector pattern.

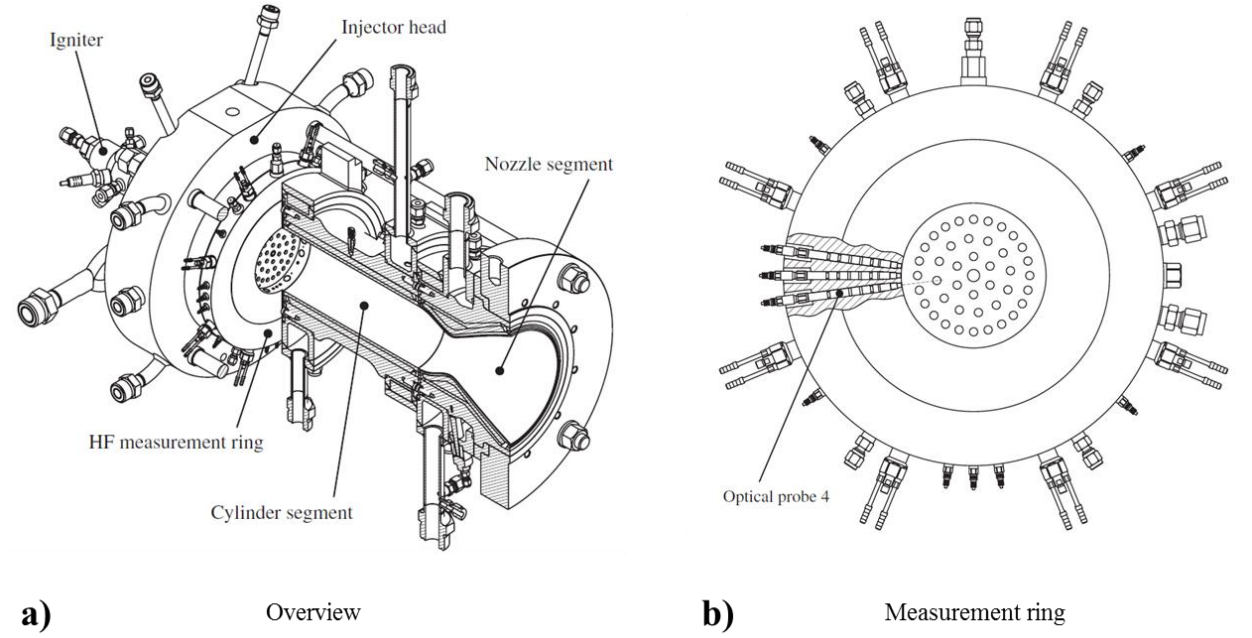

Figure 1: Research combustor BKD (HF, high frequency)

In the presented work, the results of two test runs are used. In the first test run, the combustion chamber pressure was varied in four steps of 10 bar from 80 to 50 bar. The oxidizer-to-fuel ratio was 5. The hydrogen temperature ranges between 114 and 122K, and the oxygen temperature between 113 and 117K. The load point of the second test run has a combustion chamber pressure of 70 bar with an oxydizer-to-fuel ratio of 6.8. The average hydrogen temperature was 97K and the average oxygen temperature was 123K.
The test runs used different spectrometer configurations. For the first test run, a relatively coarse grating with a spacing of 150 grooves per millimeter was used to measure a wavelength range from 290 to 430 nm, including the OH* system as well as parts of the blue radiation. With this grating, the exposure time was set to 33 ms and spectra were recorded with a sampling frequency of 20 Hz. In the second test run, the structure of the OH* system was investigated in detail. The spectrometer was equipped with a fine grating with a spacing of 3600 grooves per millimeter. To achieve higher spectral resolution of the OH system, the measured wavelength range was reduced to the range between 305.1 and 310.2 nm. For this grating, a longer exposure time of 900 ms was required and spectra were recorded with a sampling frequency of 1 Hz. All spectral data are device function corrected and smoothed by moving average.

3. Results and Discussion

The rotational temperature of OH* resembles the gas temperature for thermal equilibrium conditions [7]. Using highly resolving optical spectrographs, the rotational temperature can be derived [2,8] from the emissive decay between the two electronic states $A^2\Sigma^+$ and $X^2\Pi$ (Figure 2). However, only transitions with $\Delta v = 0$ and $v = 0$ are considered for heat release analysis. This emission band ranges over the UV regime and is explicitly examined [7]. It can be easily isolated in order to give useful information. The spectrum shows four main band heads, R_1, R_2, Q_1, and Q_2 (306.357, 306.766, 307.844 and 308.986 nm, respectively). In the temperature range between 300 and 6000K, broadening of spectral lines results mainly from the convolution of the emission spectrum with an apparatus function, which is supposed to be Gaussian with a full width at half maximum $\Delta\lambda_{app}$.

DOI: 10.13009/EUCASS2019-839

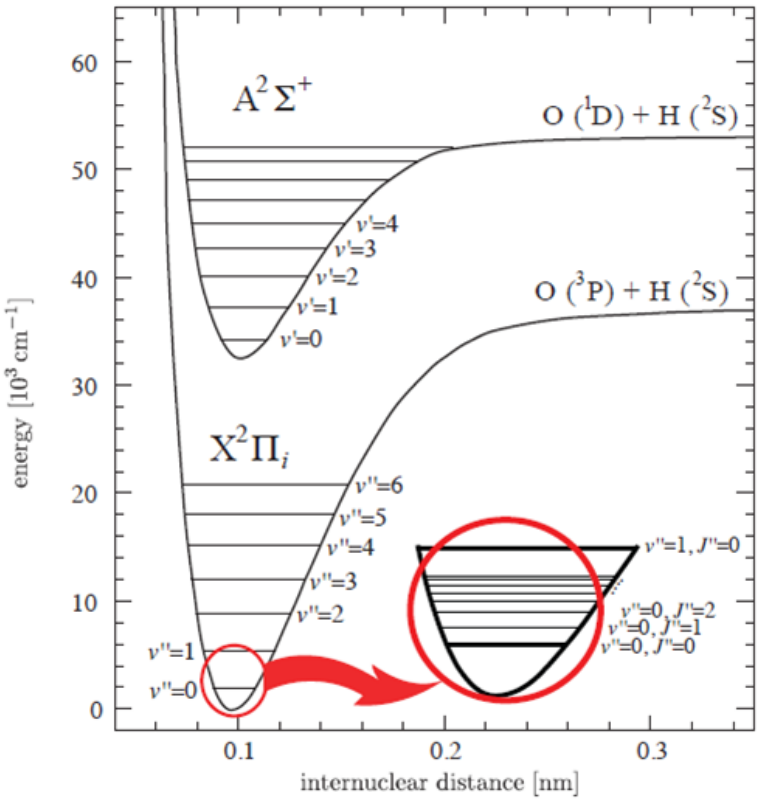

Figure 2: Electronical, vibrational and rotational energy levels of OH* [9].

The intensitiy of an individual spectral line of a band rotational structure depends on the line strength $S_{JJ'}$ for that particular line, the population of molecules in the initial state and a factor C which is the same for all lines of the same band. The intensity $I_{JJ'}$ of a particular line of rotational fine structure of the band is described as

$$I_{JJ'} = CS_{JJ'}\sigma_{JJ'}^4 \exp\left(\frac{-E_J}{k_B T}\right) \quad \textbf{(1)}$$

Where $\sigma_{JJ'}$ is the wavenumber of the transition, E_J is the rotational energy of the initial level of the line and T is the absolute temperature [10]. If no self-absorption or line superposition occurs, T can be determined from the line intensities using a Boltzmann-plot or the intensity ratio of two lines:

$$T = \frac{(E_{Jb} - E_{Ja})/k_B}{\ln\left(\frac{I_{JaJa'}}{I_{JbJb'}}\frac{\sigma_{JaJa'}^4}{\sigma_{JbJb'}^4}\frac{S_{JbJb'}}{S_{JaJa'}}\right)} \quad \textbf{(2)}$$

$$\frac{\Delta T}{T} \approx \left(\frac{\Delta R}{R} + \frac{\Delta(S_{JbJb'}/S_{JaJa'})}{S_{JbJb'}/S_{JaJa'}}\right)\frac{k_B T}{E_{Jb} - E_{Ja}} \quad \textbf{(3)}$$

$$R = \frac{I_{JaJa'}}{I_{JbJb'}} \quad \textbf{(4)}$$

However, physical limitations of the measuring spectrograph as well as turbulent flows impair the spectral results significantly. Thus, only groups of overlapping and broadened lines can be measured and hence have to be convoluted with the adequate apparatus function for simulation. Using LIFBASE [11] for calculations of OH* emission spectra, the nature of turbulent flames is revealed: As depicted in Figure 3, yet a relatively unperturbed hydrogen flame, detected in the vicinity of the injector of *BKD*, delivers less spectral resolution compared to the theoretical LIFBASE spectrum calculated with nearly the same thermodynamic parameters and the same Δλ (50 pm). Nevertheless, the spectral positions of the lines are identical for both LIFBASE and measured flame.

DOI: 10.13009/EUCASS2019-839

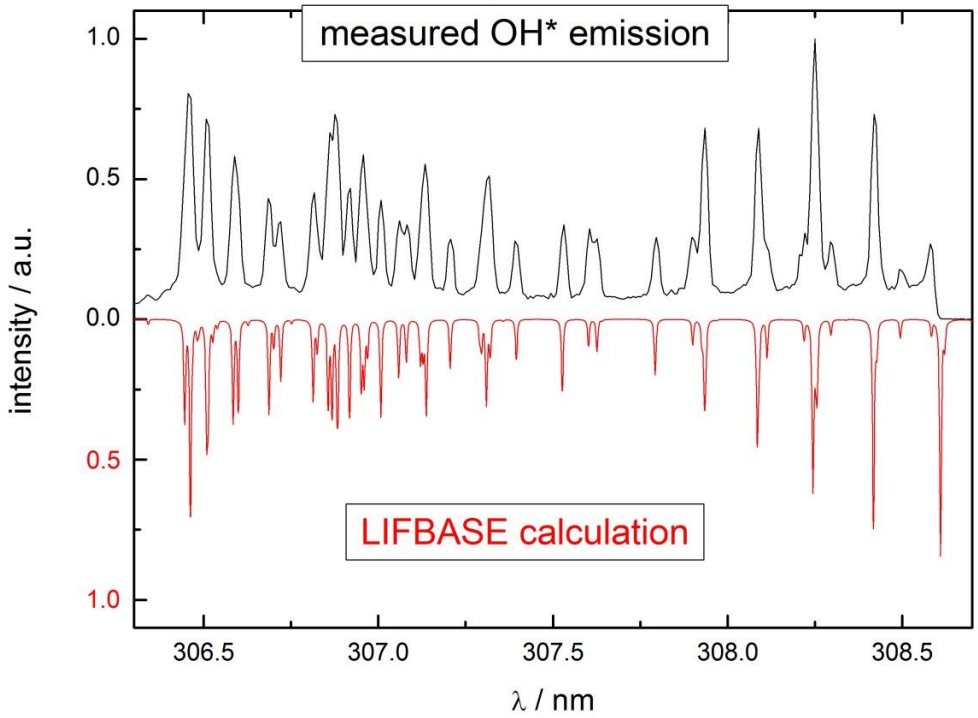

Figure 3: Comparison between a measured emission spectrum, recorded during a test run with combustion chamber D *BKD* (black) and a calculated spectrum using LIFBASE (red) with the assumption of 2000K temperature and 10 bar pressure. The spectral resolution of both graphs is ca. 50 pm. Both spectra are intensity normalized.

Spectral measurements where conducted using optical probes with several coaxial injectors in their line-of-sight. However, due to self-absorbance, only the flame emission of the outer injector contributes to the measurable data. The line-of-sight axis is located at a distance of 10 mm to the injector plate. The entrance angle for light into the optical probes is ca. 9 degrees. With the outer injector placed 20 mm away from the combustion chamber wall and therefore from the optical probe, photons of an area of ca. 2 mm^2 on the shear layer between LOX and gH_2 were collected for measurements. Sapphire as optical transparent material was used for its high value of heat conductivity as well as its thermal and pressure robustness. Furthermore, sapphire is highly transmissible in the ultra violet regime and thus extraordinarily appropriated for measuring the OH* emission.

Figure 4 shows the UV regime of the OH* emission band with the highest spectral resolution using the 3600 gr./mm grating and a Czerny Turner design spectrograph. The positions of the lines are in good agreement with data of Dieke and Crosswhite [1] as well as of the calculated LIFBASE values. Two groups of lines where used in order to correlate values of heat release with band intensities. The first one, denoted G_0, is the head band at 306.357 nm. Three maxima ($I0_1$, $I0_2$ and $I0_3$) for intensity measurement were observed after convolution. The second, denoted G_2, corresponds to the spectral range [307.844—308.532 nm], which consists of the central line Q_1 at 308.154 nm and seven maxima ($I2_1$—$I2_7$). The rotational temperature can be determined by comparison of spectral lines due to their different response on thermal energy. A selection of lines is made taking into account a variety of aspects: The maximum $I0_1$ of the G_0 group around 306.35 nm is well isolated and can be used for every temperature regime and small apparatus functions. The $I2_2$ and $I2_4$ lines of the G_2 group are also well isolated and undisturbed by other lines. The calculated ratios for *R*ij = I0i/I2j (i = 1, 2; j = 2, 4) [2] are in good agreement with measured data (Figure 6).

The temperature dependence of R_{ij} is strongly a function of the apparatus function $\Delta\lambda$ [2]. With increasing temperatures, the integrated intensity of the $I0_1$ line rises steeply for moderate temperatures and becomes saturated at high temperatures. Pellerin *et al.* [2] measured R_{ij} for apparatus functions from 0.1 nm until 20 pm with the above mentioned effect the more distinctive the lower $\Delta\lambda$. However, ethe experimental setup described here delivers an apparatus function of 7 pm, which makes it necessary to extrapolate $R_{ij}(T)$. The measured ratios $I0_1/I0_2$ and $I0_1/I2_4$ are 1.39 and 0.9, respectively, both with an uncertainty of 0.2. Correlations with temperature data give values of 2800K. Though with a relatively large uncertainty of more than 500K it is in the same order of magnitude as revealed using ANSYS CFX-2D simulations (A. Török, Figure 5) and Gordon-McBride calculations (S. Gröning, Figure 7). It shows thus a possibility to measure heat release data by taking advantage of spectral emission data.

DOI: 10.13009/EUCASS2019-839

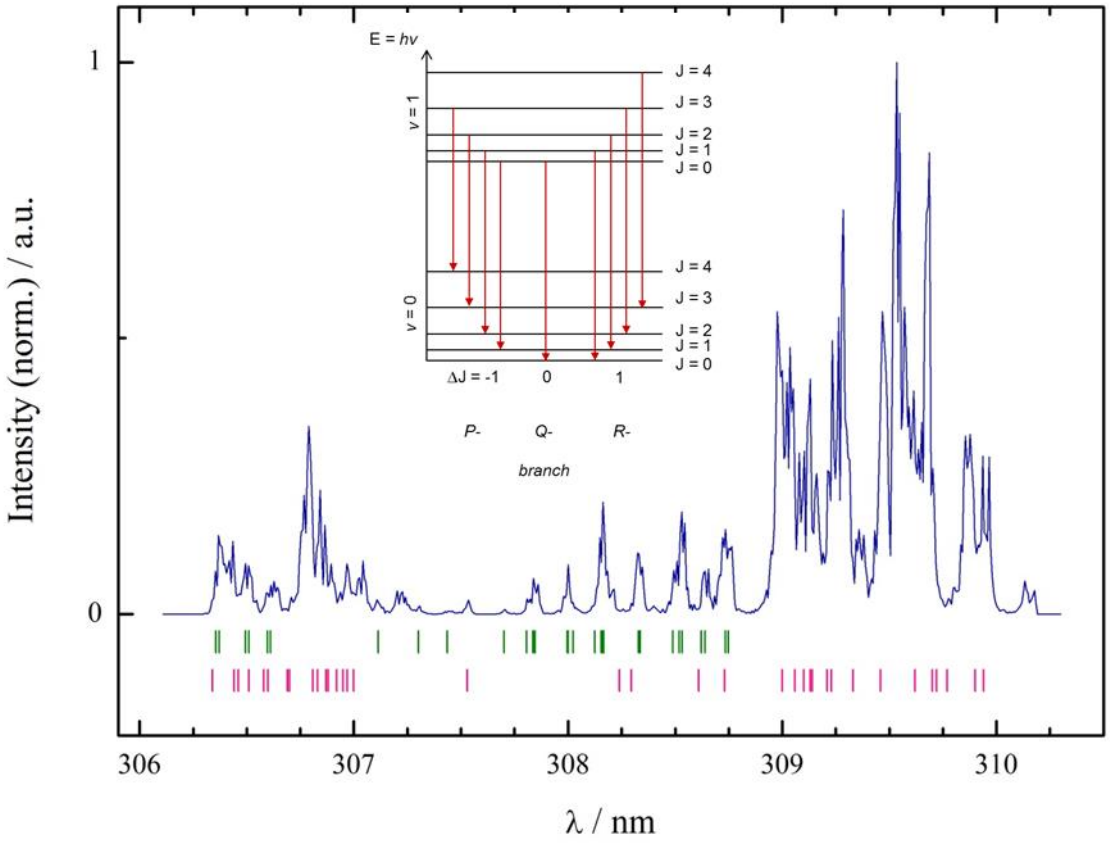

Figure 4: UV regime of the emission spectrum of OH* from combustor *D* (BKD). The green bars indicate experimentally derived reference data of Dieke and Crosswhite [7]. The purple bars indicate line positions using LIFBASE [11]. Inlay: Transition nomenclature

Pressure dependence

The pressure dependent properties of the total radiance has been determined using a laminar jet flame for pressure values, ranging from ambient up to 40 bar, and combustion chamber *D* (BKD) for pressure values from 40 bar up to 80 bar. In the case of the laminar jet flame, the total radiance is obtained by summing up the photon counts of the camera measurements with either band-pass installed. The total radiances of the jet flame are presented as a function of pressure in Figure 8. The abscissa is drawn in logarithmic scale to illustrate the strong increase of luminescence with pressure. Values above 35 bar have to be treated with care because the flame is flickering due to buoyancy at these operation conditions. This is also visible in the diagram, which presents the standard deviation of the various measurements as error bars.

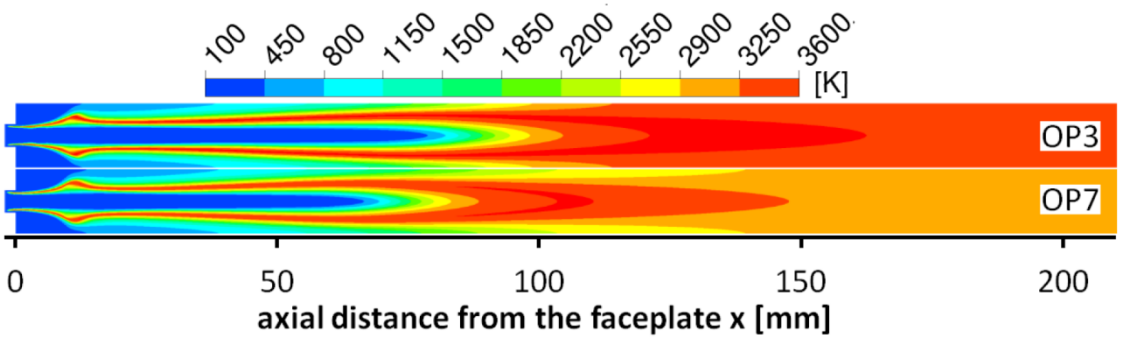

Figure 5: ANSYS CFX simulation of combustor D (BDK). Upper chart (OP3): ROF = 6; p = 80 bar. Lower chart (OP 7): ROF = 4; p = 60 bar.

DOI: 10.13009/EUCASS2019-839

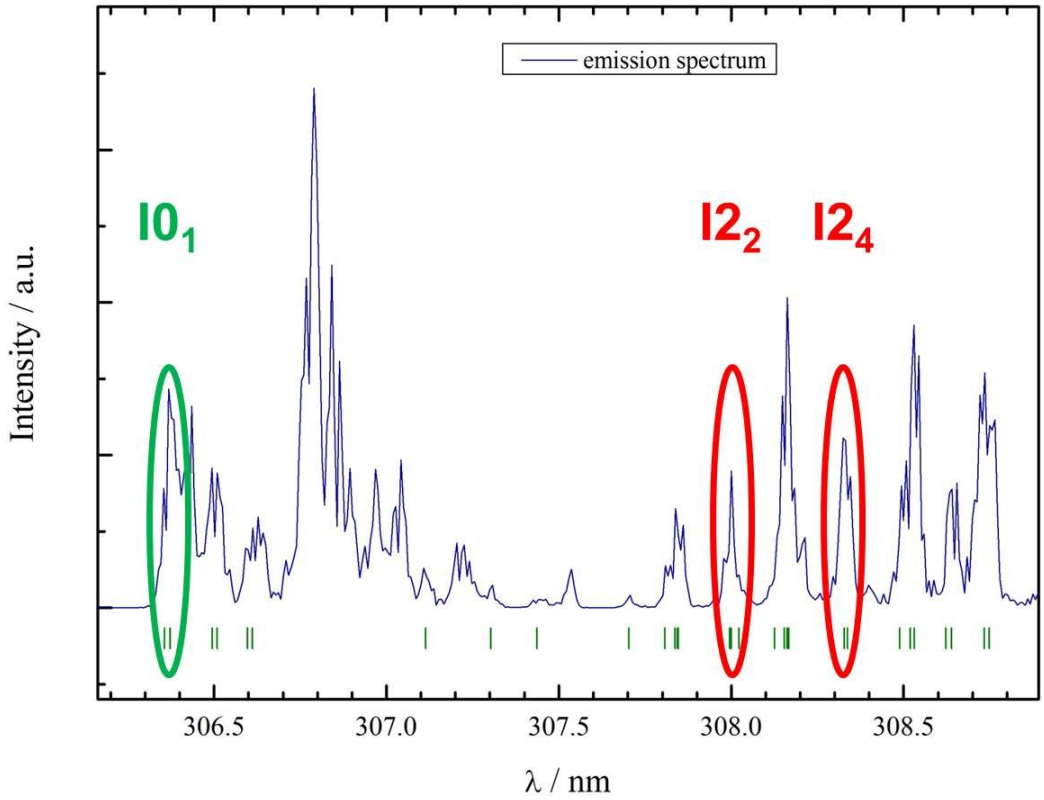

Figure 6: Relevant emission bands of the AΣ → XΠ transition in OH* from combustor *D* (BKD).

For the OH* radiation, a strong increase is observed for low pressures. This is mostly due to the increase of flame temperature with pressure, which has an exponential impact in Eq. (5). In addition, the concentration of ground-state OH, which also enhances OH* radiance, increases with the denser flame. However, due to buoyancy, the strain rate gradually increases and the flame becomes smaller [12]. The reduction of luminous area leads to the stagnation of radiance. Additionally, self-absorption prevents radiation originating from the back of the flame to reach the detector, thereby further reducing the total luminosity.

$$e_{\mathrm{OH}^*} \sim [\mathrm{OH}^*] \sim [\mathrm{OH}] \cdot \exp\left(-\frac{hc}{k_B \lambda T}\right) \tag{5}$$

The total blue radiation shows a similar dependency on pressure. However, the increase is much stronger. Whereas OH* radiation is about 40 times stronger at 30 bar compared to atmospheric pressure, the blue radiation increases by a factor of more than 1000 between 1 and 40 bar. This behaviour can be explained, if the blue radiation is assumed to originate from H2O2* chemiluminescence and reaction (6) is the dominating path of formation. The quadratic dependency of the emissivity on the OH concentration explains a stronger impact of flame density compared to the OH* radiation, which only linearly depends on the OH concentration. The reduction of luminous area due to buoyancy straining similarly causes a reduction of radiation increase. However, the blue radiation appears to steadily increase over the entire range of pressures investigated.

$$\mathrm{OH} + \mathrm{OH} \rightarrow \mathrm{H_2O_2^*} \tag{6}$$

During the experiments, the mass-flow rates of fuel and oxidizer, and, therefore, the total heat-release rate are kept constant. The strong variation of the radiances by several orders of magnitude indicates that neither type of radiation can be used as an uncorrected marker for the total heat-release rate [13].

DOI: 10.13009/EUCASS2019-839

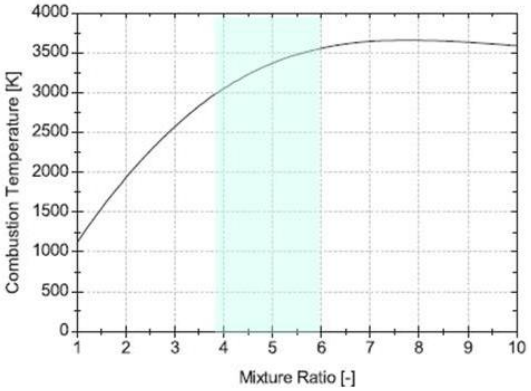

Figure 7: Calculated temperature profile for different ROF values of a LOX/gH_2 combustion [5,14]. For this study, ROF values from 4 up to 6 where used, and thus, temperature values of 3000K—3600K are expected.

In addition to the data of the laminar flame, Figure 8 also shows the OH* and blue radiances of the *BKD* flame up to 80 bar. These values correspond to the pressured dependent radiances of the emission spectrum in [12], extracted at 306 and 420 nm, respectively. The radiances are normalized by their value at 50 bar and plotted on a separate scale. The radiance of the blue radiation is multiplied by a factor of 1000 to better highlight the trend of the laminar-jet-flame data. Obviously, the highly turbulent flame in *BKD* is very different from the laminar flame. Additionally, the *BKD* measurements are only from a single line of sight and do not represent the radiation of the entire flame. A direct comparison with the laminar flame data is, therefore, not possible. Nevertheless, a relative comparison between OH* and blue radiation for the elevated pressure range can be made. Whereas OH* radiation appear to remain at an approximately constant level between 50 and 80 bar, the blue radiation increases by a factor of approximately 2. Thus, the trends observed in the laminar flame are also visible in *BKD*.

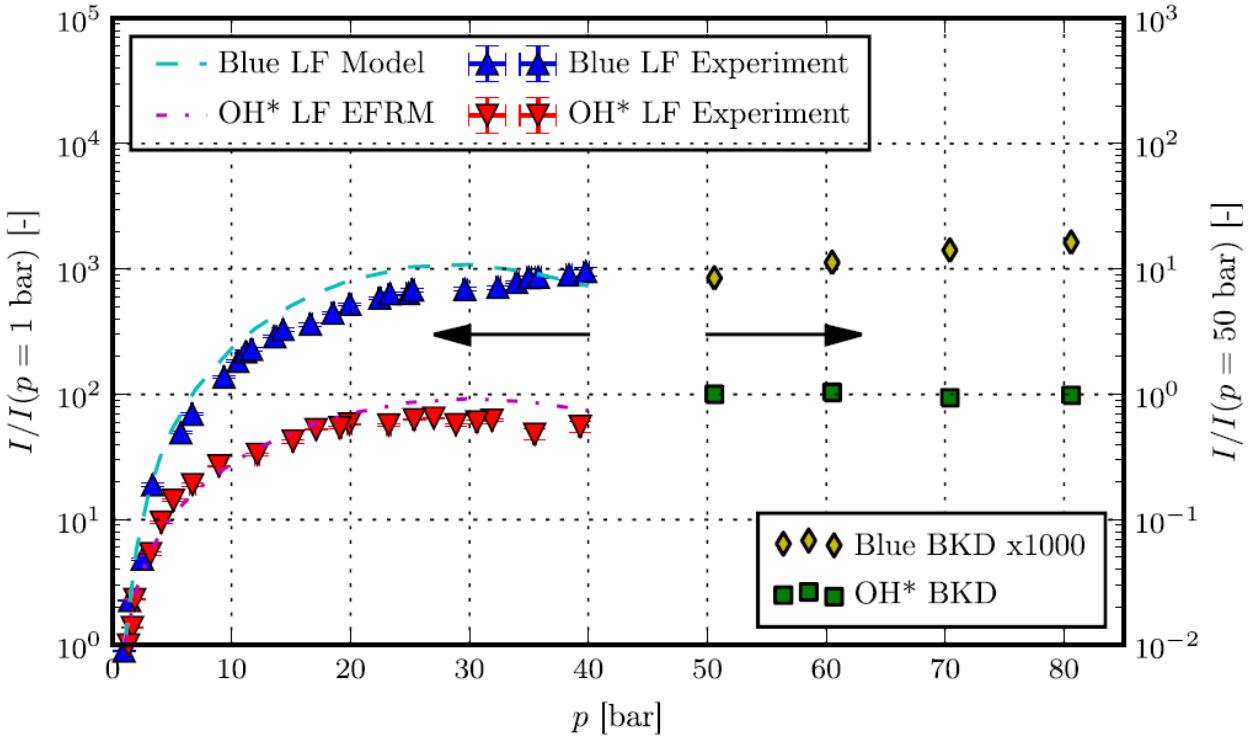

Figure 8: Total/average blue and OH* radiations (LF = laminar flame) [12].

DOI: 10.13009/EUCASS2019-839

4. Conclusion

Experiments were carried out using a high-resolution spectrograph in order to retrieve data for thermodynamic measurements during the combustion process. The feasibility of accurate measurement under harsh propulsion test conditions was shown. Stable flame emission spectroscopy enabled measuring the ultraviolet regime of the hydrogen combustion inside a research combustor (*BKD*). Taking into account the temperature-dependent nature of crucial OH* emission lines in this optical range, assumptions of the flame temperature were made.

The OH band diagnostic is available for a large temperature range. The calculated OH spectra show differences in appearance as a function of temperature. Estimation of the flame temperature can be roughly evaluated from a glance at the experimental spectrum. At room temperature the head band at 306.357 nm is not visible and only a few lines are observed. As the temperature increases, the head band intensity also increases. More accurate determination of the rotational temperature can be performed from the ratio of several head bands or isolated lines. The choice of method should be made with respect to the above analysis of possible systematic errors. Noisy spectra can also be used by taking into account a greater number of lines. Nevertheless, results obtained from R_{2j} ($j = 1\ldots3$) ratios agree well for various experimental setup, especially when using $j = 2$. Results, obtained in various experiments, show the relevance of these methods for low-temperature flame diagnostics. Generally, if an inhomogeneous state is found, temperatures and concentration gradients are observed.

Flame emission spectroscopy on a series of combustion chamber pressure values showed a similar but different behaviour for the UV and the blue regime of the hydrogen combustion. Both intensities increase with increasing pressure, but saturate for pressures beyond 80 bar.

References

[1] Dieke, G.H., and H.M. Crosswhite. 1961. The ultraviolet bands of OH. *J. Quant. Spectrosc. Radiat. Transfer*. 2 :97—199.

[2] Pellerin, S., J.M. Cormier, F. Richard, K. Musiol, and J. Chapelle. 1996. A spectroscopic diagnostic method using UV OH band spectrum. *J. Phys. D : Appl. Phys.* 29 :726—739.

[3] Haberzettl, A., D. Gundel, K. Bahlmann, J. Thomas, J. Kretschmer, and P. Vuillermoz. 2000. European Research and Technology Test Bench P8 for High Pressure and Liquid Rocket Propellants. In: *Proc. of the 36th Joint Propulsion Conference and Exhibit (JPC), Huntsville, AL.* 1—13.

[4] Suslov, D., A. Woschnak, J. Sender, and M. Oschwald. 2003. Test Specimen Design and Measurement Technique for Investigation of Heat Transfer Process in Cooling Channels of Rocket Engines Under Real Thermal Conditions. In: *Proc. of the 39th Joint Propulsion Conference and Exhibit (JPC), Huntsville, AL.* 4613.

[5] Gröning, S., J.S. Hardi, D. Suslov, and M. Oschwald. 2016. Injector-Driven Combustion Instabilities in a Hydrogen/Oxygen Rocket Combustor. *J. Propulsion and Power.* 32(3):560—573.

[6] Gröning, S., J.S. Hardi, D. Suslov, and M. Oschwald. 2015. Analysis of Phase Shift Between Oscillations of Pressure and Flame Radiation Intensity of Self-Excited Combustion Instabilities. In: *6th European Conference for Aeronautics and Space Sciences (EUCASS)*, Krakow, Poland.

[7] Dieke, G.H., and H.M. Crosswhite. 1962. The ultraviolet bands of OH. *J. Quant. Spectrosc. Radiat. Transfer.* 2:97—199.

[8] Izarra, C. de. 2000. UV OH spectrum used as a molecular pyrometer. *J. Phys. D: Appl. Phys.* 33:1697—1704.

[9] Lauer, M.R.W. 2011. Determination of the heat release distribution in turbulent flames by chemiluminescence imaging. PhD Thesis. Technical University Munich. Department for Thermodynamics.

[10] Gaydon, A.G. The spectroscopy of flames. 1957. London. Chapman & Hall. 142.

[11] Luque, J., and D.R. Crosley. 1999. LIFBASE: Database and spectral simulation version 1.5. SRI International Report MP99-009.

[12] Fiala, T., T. Sattelmayer, S. Gröning, J. Hardi, R. Stützer, S. Webster, and M. Oschwald. 2017. Comparison between excited hydroxyl radical and blue radiation from hydrogen rocket combustion. *J. Propulsion and Power*. 33(2):490—500.

[13] Fiala, T., and T. Sattelmayer. 2015. Heat release and UV-Vis radiation in non-premixed hydrogen-oxygen flames. *Exp. in Fluids*. 56(7):144.

[14] Gordon, S., and B.J. McBride. 1992. Computer Program for Calculating and Fitting Thermodynamic Functions. NASA Reference Publication 1271.